

## DEVELOPMENT LENGTH OF SAND-COATED GLASS FIBER REINFORCED POLYMER BARS WITH HEADED-END EMBEDDED IN HIGH-PERFORMANCE CONCRETE

Jennifer Lu, Khaled Sennah, and Mahmoud Sayed-Ahmed  
Department of Civil Engineering, Ryerson University, Toronto, Ontario, Canada

**Abstract:** Fiber Reinforced Polymer (FRP) bars are rapidly becoming an experienced alternative to conventional steel reinforcing bars, especially for severely exposed structures like bridges. Glass Fiber Reinforced Polymer (GFRP) bars not only exclude the durability problem associated with the corrosion of reinforcing steel bars, but also provide remarkably improved capacity due to their high tensile strength compared to that of reinforcing steel bars. First, this paper presents an experimental program on the bond strength of sand-coated GFRP bars embedded in high-performance concrete (HPC) with headed anchorage ends. Pullout tests were conducted on a few concrete blocks to study the effects of varying parameters on their bond characteristics, namely: embedment length, bar diameter and concrete. Second, an analytical investigation was conducted on the development length of the GFRP bars based on the experimental findings. And then, an expression for the development length of headed-end GFRP bars embedded in high-performance concrete was proposed.

### 1 INTRODUCTION

A few types of Fiber Reinforced Polymer (FRP) materials have been used in the construction of structures, including carbon fiber reinforced polymers (CFRP), aramid fiber reinforced polymers (AFRP), and glass fiber reinforced polymers (GFRP). However, GFRP bars are more frequently used due to their inexpensive cost relative to the other products. FRPs have many advantages that can be considered as an excellent alternative to reinforcing steel bars in many structures that subjected to severe environmental conditions such as waste water treatment and chemical plants, floating decks, bridge decks, sea walls and water structures (Masmoudi et al. 2011; Alves et al. 2011). These advantages include their non-corrosive composition, electromagnetic neutrality, high durability and high strength-to-weight ratio. This advanced reinforcing technology has high potential of improving the durability of structures; however, FRP bars are fairly new products, and there is still a lot of development and understanding of how it will endure and perform as it replaces conventional reinforcing steel bars. One critical aspect that still needs more development is the bond performance of FRP bars in concrete. The bond behavior of FRP bars performs differently than that of conventional steel reinforcement due to the different manufacturing procedures and difference in material properties in both longitudinal and transverse directions. Consequently, it is vital to study the bond characteristics of FRP bars embedded in concrete in order to develop a design standards that can be utilized by engineers.

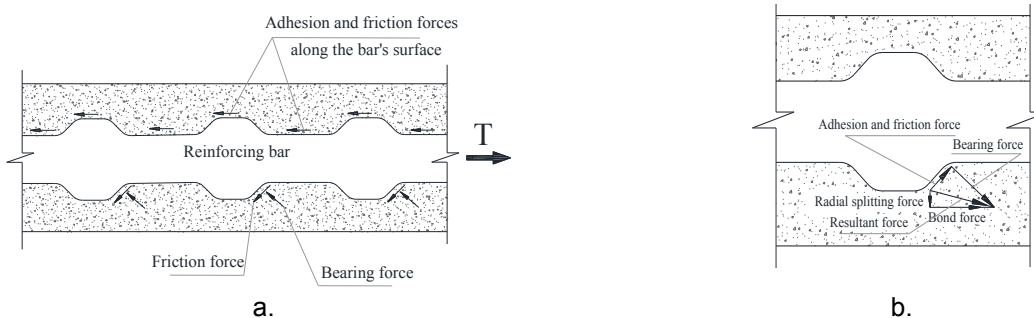


**Fig.1.** Bond force transfer mechanism at the interface between reinforcing bar and the surrounding concrete

As the transfer of stresses between the reinforcement and the surrounding concrete is mainly dependent on the quality of bond, the force transfer mechanism is always a serious issue in structural design regardless of the type of reinforcing bars (Pecce et al. 2001; Tighiouart et al. 1998). Hence, the force between the reinforcing bars and surrounding concrete should be transferred powerfully through the bond between the two materials in order to ensure strain compatibility and composite action. The transfer of forces between a reinforcing bar and concrete is owing to three different mechanisms, namely: chemical adhesion; friction and mechanical interlocking arising from the textures on the bar surface as illustrated in Fig. 1(a). The resultant of these forces can be resolved into an outward component (radial splitting force) and a shear component, parallel to the bar that is the nominal bond force as shown in Fig. 1(b). For traditional steel reinforcement, bond failure is attributed to bearing causing side splitting or shearing of concrete. On the other hand, bearing stress of the GFRP bars can exceed the shear strength between the surface deformations and the bars core resulting in a bond failure at this interface as depicted in Fig. 2(a) (Cairns and Abdullah 1996). For real structures, it is unusual for a pure pullout or pure splitting failure to occur, mostly a combination of the two modes occurs as shown in Fig. 2(b).

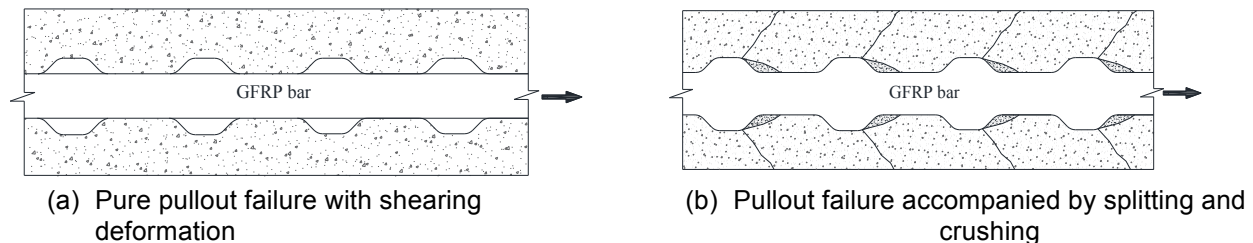


**Fig. 2.** Pullout failure modes

GFRP bars can be manufactured with various surface configurations and surface treatments in order to improve the bond action with the surrounding concrete to optimize load transfer. The different surface configurations and treatments include ribbed, spiraled wrapped, helical, and sand-coated surfaces. These are used to improve the bond between the reinforcing bar and the surrounding concrete. Morales Arias et al. (2012) suggested that sand-coated GFRP bars provided higher bond strength. Makitanit et al. (1993) noted that the sand-covered FRP bars demonstrated good bond performance due to the increased chemical bond provided by the sand particles initially, but abrupt detachment of the sand particles led to a brittle bond failure. However, Hao et al. (2009) showed that ribbed-surface GFRP bars with rib spacing equal to the bar diameter exceeded the bond strength of the sand-coated bar and exhibited a better bond-slip relationship with the least end slip at failure. Therefore, the effect of FRP surface treatment still requires more investigation.

It was also observed that the maximum average bond stress for the FRP bars decreased with an increase in the embedment length as exhibited by steel bars (Ametrano 2011; Firas et al. 2009; Pecce et al. 2001; Tighiouart et al. 1998). Due to the nonlinear distribution of the bond stress along the length of the reinforcing bar, as the embedment length increases, the stress is distributed over a longer length and henceforth, the bond strength decreases. Ametrano (2011) conducted both beam and pullout tests with sand-coated GFRP bars embedded in high strength and ultra-high performance concrete, which both demonstrated a decrease in bond strength as the embedment length increased. In addition, bond failure mechanism of FRP bars in concrete is influenced by concrete cover around the reinforcing bar by virtue of its confining effect (Galati et al. 2006; Ehsani et al. 1997 and 1993). Regression manipulation on different experimental results indicated that good correlation exists between bond strength and the square root of the compressive strength of concrete (CSA S806 2012; ACI 440.1R 2006; Okelo and Yuan 2005). Achillides and Pilakoutas (2004) demonstrated that for the case of concrete strength greater than 30 MPa, bond failure occurred partly on the surface of the GFRP bar and in the concrete. Baena et al. (2009) explained that the bond strength of the FRP bar does not depend on the concrete strength, but rather on the GFRP bar's properties.

In 1993, the Federal Highway Administration, FHWA, in USA introduced high performance concrete (HPC) designation for the use in bridge construction with eight performance characteristics; four for the



concrete durability and four for its strength. The definition consisted of four durability characteristics that include freeze-thaw resistance, scaling resistance, abrasion resistance and chloride penetration, while the four strength characteristics include compressive strength, modulus of elasticity, drying shrinkage and creep. High strength concrete (HSC) allows the use of longer span lengths, wider girder spacing, shallow girders, or their combination resulting in economical structures. ACI defined HPC as the concrete that has the compressive strength of 55.16 MPa or greater (ACI Committee 363-2010). AASHTO-LRFD Bridge Construction Specification (AASHTO 2012) included two class of HPC designated as P(HPC) for prestressed elements with strength greater than 41.37 MPa and A(HPC) for cast-in-place (CIP) construction with strength less than or equal to 41.37 MPa. HPC is composed of supplementary cementitious materials (SCM) including cement, fly ash, silica fume and slag cement. Water-cement (w/cm) ratio is used to represent the weight of water to the binding materials. In 1987, the Strategic Highway Research Program (SHRP) proposed the mechanical behavior of the HPC to be: (i) maximum w/cm ratio of 0.35, (ii) minimum durability factor of 80% as determined by ASTM C666\_Method A, (iii) minimum compressive strength of 20.69 MPa within 4 hours after placement, 34.48 MPa within 24 hours, and 68.95 MPa within 28 days.

In 2006, the Federal Highway Administration in USA, FHWA, proposed new revision for eleven characteristics and three grades of performances of HPC. The eleven performance characteristics include: freeze-thaw (F/T) durability; scaling resistance (SR); abrasion resistance (AR); chloride penetration (CP); alkali-silica reactivity (ASR); sulfate resistance (SR); flowability; strength; elasticity; drying shrinkage; and creep. SCM limited the use of Type III cement in only precast concrete members. Fly ash of Class C, F or N pozzolan is used with upper limits of 15% to 30% of the total cementitious materials. Silica fume is restricted to an upper limit that range from 7% to 10% and lower limit of 5% to 7% of the total cementitious materials. The use of slag cement has upper limit of 30% to 50% of the total cementitious materials. The aggregate for concrete bridge decks is the normal weight aggregate conforming to AASHTO Specifications M6 and M80, or the lightweight aggregate conforming AASHTO M195, or the combination of them. AASHTO Specifications M6 and M43 contain the grade specifications for the coarse normal weight aggregates. Chemical admixtures conforming to AASHTO M194 or ASTM C494 through its seven types of admixtures (A through G) are permitted.

The main objectives of the current study were to conduct a parametric study on the effect of different parameters on the bond characteristics of glass fiber reinforced polymer (GFRP) bars with headed-end embedded in high performance concrete (HPC). Hence, the development length for both sand-coated GFRP bars could be determined based on the experimental findings. In order to increase the reliability of experimental findings, test results of each studied parameter was obtained based on characteristic value of the pullout strength of five identical specimens. It should be noted that the characteristic strength takes into account the number of individual specimens and the deviation of the strength value of each specimen with the mean. As a consequence, the pullout test was performed on 45 specimens in order to cover the effect of different parameters on the bond strength. The parametric study included bar diameter, embedment length and concrete cover. Finally, an expression for the development length calculation was developed for sand-coated GFRP bars with headed ends.

## 2 EXPERIMENTAL TEST PROGRAM

In total, 45 pullout specimens with headed-end sand-coated GFRP bars were cast and tested. Concrete cover of 40 and 60 mm were used in this study. The effect of bar diameter was examined considering two separate bar diameters of 15.875 and 19.050 mm, with anchorage heads of exterior diameters of 47.625 mm and 57.150 mm, respectively. The effect of embedment length on bond strength was investigated considering two different lengths of, firstly, the length of the anchorage head ( $0d_b$ ) and, secondly, the length of the anchorage head and four times the bar diameter ( $4d_b$ ). For all varying parameters, five identical specimens were cast and tested in order to increase the reliability of the test findings. The configuration of the pullout test specimens consisted of GFRP bars embedded into concrete blocks. The concrete blocks had a base dimension of 300 mm length with varying heights depending on the varying embedment lengths. Figs. 3(a) and 3(b) show the details of the dimensions of the pullout test specimens for both concentric and eccentric configuration. The used concrete was high-performance ready mix

concrete (HPC) with target concrete cylinder strength of 70 MP, while the characteristic compressive strength of concrete obtained from concrete cylinders was 65 MPa. In this research, sand-coated bars, shown in Fig. 3(c) (Pultrall 2014) was used. The nominal tensile modulus for the sand-coated GFRP bars was 60 GPa for both straight-end and headed-end types. The maximum exterior diameters of the anchorage heads were 3 times the diameter of the bar, with the head length of approximately 100. The purpose of the anchorage head is to provide a strong anchoring system and avoid splitting mechanism around the anchorage head. Bar lengths of 1500 mm were used in order to allow for the installation of a grip system for pullout testing of the specimen.

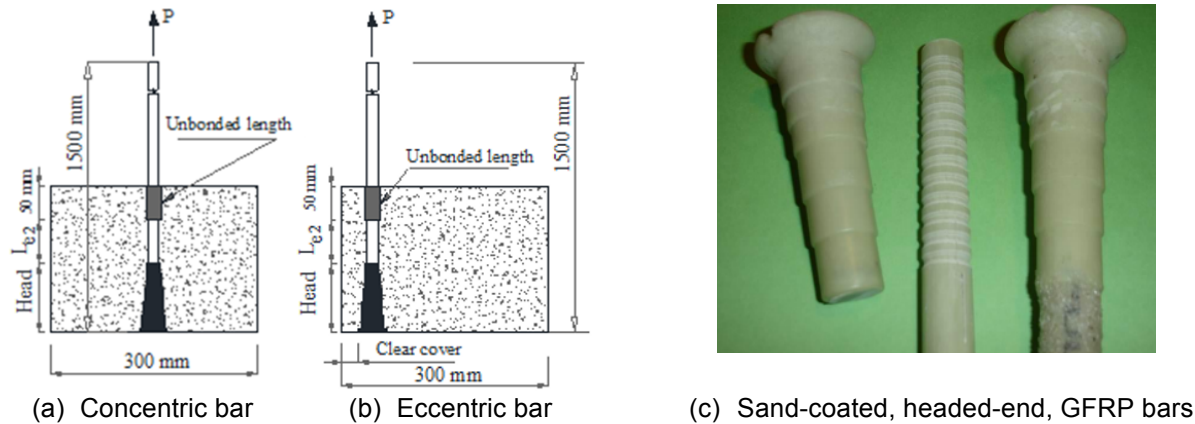


Fig. 3. Details for test specimens

## 2.1 Test Setup, Test Procedure and Instrumentation

The type of pullout testing undertaken in this research is called confined pullout testing, since the top of concrete is under bearing compression from the bearing plate. This would prevent concrete cones to form on top of concrete at failure (CAN/CSA-A23.3-04). The main requirement specified in CSA-S807 standard for this type of testing is that the grip distance should be at least  $40d_b$ , where  $d_b$  is the bar diameter. This limitation was considered in all test setups. In addition, all pullout tests were performed according to the CAN/CSA S806-12 test equipment and requirements. Figure 4(a) shows a schematic diagram for the pullout test setup, while Fig. 4(b) shows a photo for the setup. The test setup consisted of 4 steel plates, a loading cell, and the grip system. The steel plates had a total thickness of 62.5 mm, and they were placed in a position to distribute the compression reaction on the specimen face. The loading cell was attached to a computer data acquisition system to record the applied jacking load. A hydraulic jack with an aluminum hollow plunger cylinder was used to exert the tensile force on the specimen's GFRP bar. The grip system was a standard wedge type grip system. The wedges had specific grooving patterns to allow full contact with the GFRP bars, which helped minimizing localized transverse stress and reducing the prohibiting of premature damage in the bar itself. A hollow steel tube with inside conical surface shape was the support system for the three wedges that were used to grip the GFRP bar. For this research, special wedges were manufactured for each of the #5 and #6 bars, 16/15.875 mm and 20/19.050 mm GFRP bars, respectively. For each specimen, the hollow steel tube was sprayed with graphite as lubricate for easy insert and removal of the three wedges at the beginning and end of the pullout test. The steel wedges were then carefully hammered into place, surrounding the bar. It was important that the bar was in the center of the hollow tube and that the steel wedges were equally spaced out so that the bar would experience equal stress all around its circumference. After each test, the residue on the wedges from the previous bar was cleaned off to ensure proper grip was achieved for further tests.

For each pullout test, free-end slip and loaded-end slip were recorded with Linear Variable Differential Transformers (LVDTs). The LVDTs had to be carefully positioned at the center of the GFRP bar. A steel bracket and a 400 mm deep-throat bar clamp were used to clamp the LVDT in position as shown in Fig. 3(d). As for the loaded-end slip measurement, the LVDT was placed parallel to the grip system and the measurements were taken with the end of the hollow plunger cylinder as the reference point, as shown in Fig. 3(e). After assembling the test setup, the pullout test was performed by applying the pullout load at a

specified rate using the hydraulic jack operated in open loop control. The load was applied to the GFRP bar at a rate not greater than 22 kN/min, while the free end slip was recorded with accuracy 0.001 mm per CAN/CSA S806-12. The data from the load cell and LVDTs were recorded using test control software (TCS) with a data acquisition unit. The data acquisition system recorded the applied load with a precision of 0.01 kN. According to the CAN/CSA S806-12 pullout test requirements, the test was terminated when one of the following conditions occurred: (a) the FRP bar ruptured; or (b) the FRP bar slipped a distance at least equal to its diameter.

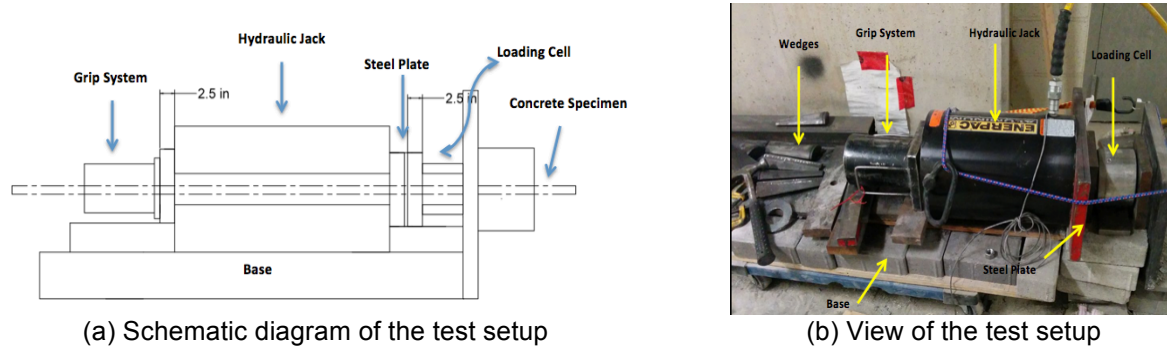


Fig. 4. Pullout test setup

## 2.2 Specimen Nomenclature

The specimen nomenclature for straight-end bars consists of either 3 or 4 symbols separated by a dash as depicted in Tables 1 and 2 that record the experimental and theoretical findings of this research. The concentric bars have 3 symbols, while the eccentric bars have 4 symbols. The first symbol indicates the bar size (H5 = 15.875 mm, H6 = 19.05 mm) where H stands for headed-end. The second nomenclature stands for either embedment length for concentric bars (C64) or the value of the eccentricity for eccentric bars (60E for 60 mm concrete cover and 40E for 40 mm concrete cover). In the meantime, the third nomenclature after 60E or 40E represents the embedment length for the eccentric bars. The last nomenclature stands for the type of the used bars (V stands for V-Rod sand-coated bars).

## 3 RESULTS AND DISCUSSIONS

Table 1 presents the test results for sand-coated bars with headed ends. The average loads for each 5 identical specimens are presented as well as the dominant mode of failure. In the current study, the characteristic pullout loads are used instead of the average pullout loads in order to account for the variation of the actual failure loads for each specimen as affected by the number of tested specimens and variation of the strength value of each specimen from the mean. According to CAN/CSA S807-10, the characteristic pullout load can be calculated using Eq. (1).

$$[1] \quad F_t = \left( \frac{1 - 1.645V}{1 + \frac{1.645V}{\sqrt{n}}} \right) \cdot F_{av}$$

Where  $F_t$  = the characteristic failure load (kN);  $F_{av}$  = the average failure load (kN);  $n$  = number of samples = 5;  $V$  = coefficient of variation of failure loads.

Table 1 shows the characteristic failure load as well as the average failure load for each parameter. It can be noted that the characteristic failure loads range from 0.60 to 0.95 times the average failure loads. The higher value corresponds to the smaller variation among the failure loads within each identical specimens, while the lower value corresponds to larger variation among the failure loads. The average bond stress along the embedded length for each specimen was calculated using Eq. (2).

$$[2] \quad \tau = \frac{F}{\pi d_b h_e}$$

Where  $\tau$  = average bond stress (MPa);  $F$  = applied failure load (N);  $d_b$  = bar diameter (mm) and  $h_e$  = embedment length considering the head length (mm). In this part, test results are presented and analyzed

in details for the manifested modes of failure for headed-end GFRP bars, the effect of the surface condition on the bond stress and the development length calculation. Other parameters such as bond-slip relationship and the effect of different parameters on the bond stress for the tested bars are analyzed in details elsewhere (Lu 2014). In general, a gradual drop in bond stress was experienced with increase in embedment length, which is similar to the behavior experienced in other researchers' findings. Generally, the increase of concrete cover yielded higher bond stress. Table 1 showed similar trend of results for different parameters on the bond stress of headed-end sand-coated GFRP bars. However, all specimens experienced either failure at head anchorage or at the interface between the bar's end and its anchorage.

**Table 1.** Test result for sand-coated GFRP bars with headed-ends

Specimen notation	Embedment length, mm	Average ultimate load, kN	Characteristic load, kN	COV	(4)/(3)	Average bond stress, MPa	Dominant mode of failure
(1)	(2)	(3)	(4)	(5)	(6)	(7)	(8)
H5-C-0-V	100	105.65	94.21	0.047	0.89	11.52	BS
H5-C-64-V	164	113.00	67.71	0.187	0.60	13.58	BS
H5-40E-0-V	100	94.40	85.46	0.041	0.91	17.14	BS-CCS
H5-40E-64-V	164	128.15	93.48	0.124	0.73	11.43	BS-VSCCC
H5-60E-0-V	100	142.63	109.50	0.102	0.77	21.96	BS-CS
H5-60E-64-V	164	130.56	90.24	0.140	0.69	11.03	BS-CS
H6-C-0-V	100	162.30	103.56	0.171	0.64	17.36	HB-BS-CS
H6-C-76-V	176	222.00	210.34	0.019	0.95	19.99	HB-BS-CS
H6-40E-0-V	100	91.42	72.53	0.086	0.79	12.12	HB-BS-CS
H6-40E-76-V	176	138.95	93.93	0.151	0.68	8.92	BS-CS

COV: coefficient of variation; BS: Bar slippage from the head; BS-CCS: Bar slippage from the head and concrete cover splitting; BS-VSCCC: Bar slippage from the head and V-shape side concrete cover crack; BS-CS: Bar slippage from the head followed by concrete splitting; HB-BS-CS: Bar head breakage followed bar slippage and concrete splitting.

### 3.1 Modes of Failure

Figures 5 and 6 show the failure modes for concrete blocks with concentric and eccentric sand-coated GFRP bars with headed ends, respectively. For the concrete blocks with concentrically positioned GFRP bars, the common failure mode was either bar slippage from the head (BS) or bar head breakage followed by bar slippage and concrete splitting (HB-BS-CS) as depicted in Fig. 5. As for concrete blocks with eccentric GFRP bars, three common failure modes were noted, namely: bar slippage from the anchorage head followed by concrete splitting (BS-CS) as depicted in Fig. 6(a), bar slippage from the anchorage head followed by a V-notch side concrete crack (BS-VSCCC) as depicted in Fig. 6(b), and bar slippage from the anchorage head and concrete cover splitting (BS-CCS) as shown in Fig. 6(c).

For the concentric bars, two types of failure were observed in the bar head. The first type of failure happened when the bar head was broken at the largest desk near the bar end, as depicted in Fig. 5(a), at a force exceeding the tensile rupture strength of the material forming the head, followed by concrete splitting. The second type of failure occurred when the bar slips from the anchorage head at a force exceeding the shear strength between the bar itself and anchorage head, causing a longitudinal crack in the head, followed by concrete splitting through the entire specimen as depicted in Fig. 5(b). The length of the anchorage head serves a similar role as the embedment length of straight bars. Also, the anchorage head provides an additional wedging effect that allows the headed specimens to achieve similar bond strength to straight-ended specimens with longer embedment lengths. Thus, this finding confirms that the anchorage head provides adequate adhesive bond properties and is the main component to achieve the successful bond mechanism.



(a) Bar head breakage followed by bar slippage and concrete splitting (HB-BS-CS)



(a) Bar slippage from the anchorage head followed by concrete splitting (BS-CS)



(c) Bar slippage from the anchorage head and concrete cover splitting in case of zero embedment length with bar head in case of #6 GFRP bar (BS-CCS)



(b) Bar head breakage through a longitudinal crack followed by bar slippage and concrete splitting (HB-BS-CS)



(b) Bar slippage from the anchorage head and V-shape side concrete cover crack in case of embedment length of 76 mm with bar head in case of #6 GFRP Bar (BS-VSCCC)



**Fig. 5.** Failure modes for concrete blocks with concentric sand-coated GFRP bars with headed-ends.

**Fig. 6.** Failure modes for concrete blocks with eccentric sand-coated GFRP bars with headed-ends.

For the eccentric GFRP bars, three types of failure were observed in the bar head. The first type of failure is depicted in Fig. 6(a) on which the bar slips from the head followed by concrete splitting. The left image in Fig. 6(a) shows the portion of the bar to the right of head slipped off the head. Also, the image shows that the straight portion of the embedment length outside the bar has the sand-coating sheared off the bar core as an indication of bar slippage. Similar observation is depicted in right image in Fig. 6(b). The second and third failure modes shown in Fig. 6(b) and (c) are identical to the first failure mode depicted in Fig. 6(a) except that concrete splitting was due to V-notch side concrete cover crack and concrete cover splitting, respectively.

### 3.2 Development Length of GFRP Bars

Equation (3) provides the relationship between the average bond stress and the corresponding embedment length under the effect of the applied pullout load. The development length is defined as the minimum length required to fully develop the design tensile stress in the GFRP bars. Using the design value of the tensile strength of the GFRP bars for sand-coated GFRP bars, Eq. (3) can be rewritten as follows:

$$[3] \quad \tau = \frac{A_b f_t}{\pi d_b l_d}$$

Where,  $\tau$  = average bond stress (MPa);  $f_t$  = design tensile strength of the GFRP bars (MPa);  $d_b$  = bar diameter (mm);  $A_b$  = cross-sectional area of the bar (mm<sup>2</sup>) and  $l_d$  = development length. From Eq. (3), development length can be calculated as follows:

$$[4] \quad l_d = \frac{A_b f_t}{\pi d_b \tau} = \frac{d_b f_t}{4\tau}$$

Since previous studies indicated that good correlation exists between the bond strength and the square root of the compressive strength of concrete (ACI 440.1R-06; Okelo and Yuan 2005) besides the bond stress is inversely proportional to the bar diameter size, the bond stress can be represented by Eq. (5) (Hao et al. 2006; Okelo and Yuan 2005; Achillides and Pilakoutas 2004; Tighiouart et al. 1998).



$$[5] \quad \tau = A \frac{\sqrt{f'_c}}{d_b}$$

Where,  $f'_c$  = concrete compressive cylinder strength (MPa) and constant  $A$  can be determined based on experimental results. Hence, Eq. (5) can be rewritten as follows:

$$[6] \quad l_d = \frac{d_b^2 f_t}{4A \sqrt{f'_c}}$$

Equation (7) can be rewritten in the following form:

$$[7] \quad l_d = B \frac{d_b f_t}{\sqrt{f'_c}}$$

Where

$$[8] \quad B = \frac{d_b}{4A} = \frac{\sqrt{f'_c}}{4\tau}$$

Table 2 Development length parameters of sand-coated GFRP bars with headed-ends

Specimen notation	Embedment length, mm	Bar diameter, mm	Characteristic load, kN	Average bond stress, MPa	Bond factor, B	Average tensile stress, MPa	Development length, mm
H5-C-0-V	100	15.875	94.21	11.52	0.176	476.05	407.90
H5-C-64-V	164	15.875	67.71	13.58	0.149	342.14	346.02
H5-40E-0-V	100	15.875	85.46	17.14	0.118	431.83	274.15
H5-40E-64-V	164	15.875	93.48	11.43	0.178	472.36	411.11
H5-60E-0-V	100	15.875	109.50	21.96	0.092	553.31	213.98
H5-60E-64-V	164	15.875	90.24	11.03	0.184	455.99	426.02
H6-C-0-V	100	19.050	103.56	17.36	0.117	363.37	303.14
H6-C-76-V	176	19.050	210.34	19.99	0.102	738.04	263.26
H6-40E-0-V	100	19.050	72.53	12.12	0.167	254.49	434.20
H6-40E-76-V	176	19.050	93.93	8.92	0.228	329.58	589.97

Tables 2 summarizes the development length parameters the headed-end GFRP bars. It can be noticed that the actual stresses for headed-end GFRP bars are lower than the design values. Thus, in order to enable these bars to exhaust their design tensile strength, the embedment lengths had to be increased as manifested by the comparison between the embedment length and the development length. Based on the calculated values, the constant  $B$  should be selected in such a way that the resulting equation yields a conservative value of the development length. Consequently, constant  $B$  used in Eq. (8) can be suggested as follows:

$$[9] \quad B = 0.188 + \frac{l_{e2}}{100 d_b} \quad (\text{For headed-end sand coated bars})$$

Where  $l_{e2}$  = the additional straight part of the bar to the head as a multiplier of the bar diameter. Thus, the development length for straight- and headed-end GFRP bars embedded in high-strength concrete can be proposed as follows:

$$[10] \quad l_d = \left( 0.188 + \frac{l_{e2}}{100 d_b} \right) \cdot \frac{d_b f_t}{\sqrt{f'_c}} \quad (\text{For headed-end sand-coated bars})$$

#### 4 CONCLUSIONS

This paper presented a parametric study on the effect of the controlling variables on the bond behavior of sand-coated GFRP bars with headed ends cast in high-performance concrete (HPC) with a characteristic





concrete compressive strength of 65.94 MPa, aiming to determine the basic experimental development lengths. The controlling variables, included bar diameter, concrete cover dimensions and embedment length. Although results of the tested headed-end bar specimens showed scattered data as a result of the head breakage and bar slippage from the head, statistical analysis was conducted to develop an empirical equation of the development length limit of sand-coated GFRP bars with headed-end cast in HPC for use by design engineers and design code writers.

### Acknowledgements

This study was sponsored by Ontario Ministry of Transportation's (MTO) Highway Infrastructure Innovation Funding Program through cash contribution, St. Marys / Canada Building Materials (CBM) of Toronto, Ontario, Canada, through supplying HPC, and Pultrall Inc. through providing GFRP bars. Such research contribution is very much appreciated. Special thanks to Mr. Philip Zacarias, Technical Services Manager of CBM, for assisting in supplying HPC. Opinions expressed in this paper are those of the authors and do not necessarily reflect the views and policies of the Ministry or other partners.

### References

- AASHTO 2012. AASHTO LRFD Bridge Design Specifications, Customary U.S. Units. American Association of State Highway and Transportation Officials, Sixth Edition.
- Achillides, Z., and Pilakoutas, K. 2004. Bond behaviour of fibre reinforced polymer bars under direct pullout conditions. *J. Compos. Constr.*, 8, 173-181.
- ACI Committee 363. 2010. Report on High-Strength Concrete. *ACI 363R-10*, American Concrete Institute Committee 363, Farmington Hills, MI.
- ACI Committee 440. 2006. Guide for the Design and Construction of Structural Concrete Reinforced with FRP Bars. *ACI 440.1R-06*, Farmington Hills, MI.
- Alves, J., El-Ragaby, A., and El-Salakawy, E. 2011. Durability of GFRP bars' bond to concrete under different loading and environmental conditions. *J. Compos. Constr.*, 15(3), 249-262.
- Ametrano, D. 2011. Bond characteristics of glass fibre reinforced polymer bars embedded in high strength and ultra-high performance concrete. Master of Applied Science, Ryerson University, Civil Engineering, Toronto.
- Baena, M., Torres L. L., Turon A., and Barris, C. 2009. Experimental study of bond behavior between concrete and FRP bars using a pull-out test. *Compos: Part B*, 40, 784-797.
- Cairns, J., and Abdullah, R. B. 1996. Bond strength of black and epoxy-coated reinforcement: A theoretical approach. *ACI Mater. J.*, 93(4), 362-369.
- CAN/CSA S806-12. 2012. Design and construction of building components with fibre reinforced polymers. Canadian Standards Association. Rexdale, Ontario, Canada.
- CAN/CSA-A23.3-04 (R2010). 2010 Design of concrete structures. Canadian Standard Association, Toronto, Ontario, Canada, 258p.
- CAN/CSA S807-10. 2010. Specification for fiber-reinforced polymers." Canadian Standard Association, 44p.
- CAN/CSA-S6-06. 2006. Canadian highway bridge design code. Canadian Standards Association, Toronto, Ontario, Canada.
- Ehsani, M. R., Saadatmanesh, H., and Tao, S. 1993. Bond of GFRP rebars to ordinary-strength concrete. *ACI Int. Symp.*, on Non-Metallic Continuous Reinforcement, Vancouver, Canada, 333-345.
- Ehsani, M., Saadatmanesh, H., and Tao, S. 1997. Bond behaviour of deformed GFRP bar. *J. Compos. Mater.*, 31 (14), 1413-1430.
- Firas, S., Gilles, F., and Le Roy, R. 2009. Bond between carbon fibre-reinforced polymer (CFRP) bars and ultra high performance fibre reinforced concrete (UHPFRC). *Constr. & Build. Mater.*, 479-485.
- Galati, N., Nanni, A., Dharani, L., Focacci, F., Aiello, A. 2006. Thermal effects on bond between FRP rebars and concrete." *Compos. Part A*, 37, 1223-1230.
- Hao, Q., Wang, Y., He, Z., and Ou, J. 2009. Bond strength of glass fiber reinforced polymer ribbed rebars in normal strength concrete. *Constr. & Build. Mater.*, 23 (2), 865-871.
- Lu, J. 2014. Investigation of pullout strength of pre-installed glass fiber reinforced polymer bars in high-performance concrete. Master of Engineering Project, Civil Engineering Department, Ryerson University, Toronto, ON, Canada, 2014.



- Makitani, E., Irisawa, I., and Nishiura, N. 1993. Investigation of bond in concrete member with fiber reinforced plastic bars. *Proc. Int. Symp. on Fibre-Reinforced-Plastic Reinforcement for Concrete Structure*, A. Nanni, & C. Dola, Eds., 315-331.
- Masmoudi, R., Masmoudi, A., Ouezdou, M., and Daoud, A. 2011. Long-term bond performance of GFRP bars in concrete under temperature ranging from 20 °C to 80 °C. *Constr. & Build. Mater.*, 25, 486–493.
- Morales Arias, J., Vazques, A., and Escobar, M. 2012. Use of sand coating to improve bonding between GFRP bars and concrete. *J. Compos. Mater.*, 46 (18), 2271-2278.
- Okelo, R., and Yuan, R. L. 2005. Bond strength of fibre reinforced polymer rebars in normal strength concrete. *J. Compos. Constr.*, 9(3), 203-213.
- Pecce, M., Manfredi, G., Realfonzo, R., and Cosenza, E. 2001. Experimental and analytical evaluation of bond properties of GFRP bars. *J. Mater. in Civil Eng.*, 13(4), 282-290.
- Pultrall Inc. 2014. V-ROD properties. Downloads retrieved on May 23, 2014, <http://www.vrod.ca/en/downloads.asp>.
- Tighiouart, B., Benmokrane, B., and Gao, D. 1998. Investigation of bond in concrete member with fibre reinforced polymer (FRP) bars. *Constr. Build. Mater.*, 12(8), 453-462.